Supplementary Information

From 20% Single-Junction Organic Photovoltaic to 26% Perovskite/Organic Tandem Solar Cells: Self-Assembled Hole Transport Molecules Matters

Xiaokang Sun,‡[ab] Fei Wang,‡[a] Guo Yang,‡[a] Xiaoman Ding,[a] Jie Lv,[a] Yonggui Sun,[a] Taomiao Wang,[a] Chuanlin Gao,[c] Guangye Zhang,[c] Wenzhu Liu,[d] Xiang Xu,[a] Soumitra Satapathi,[e] Xiaoping Ouyang,[b] Annie Ng,*[f] Long Ye,[g] Mingjian Yuan,[h] Hongyu Zhang,*[i] Hanlin Hu*[a]

[a] Hoffmann Institute of Advanced Materials, Shenzhen Polytechnic University, 7098 Liuxian Boulevard, Shenzhen 518055, China

E-mail: hanlinhu@szpu.edu.cn

[b] School of Materials Science and Engineering, Xiangtan University, Xiangtan 411105, China

[c] College of New Materials and New Energies, Shenzhen Technology University, Shenzhen, 518118, China

[d] Research Center for New Energy Technology, Shanghai Institute of Microsystem and Information Technology, Chinese Academy of Sciences, Shanghai, China.

[e] Indian Institute of Technology Roorkee, Uttarakhand 247667, India

[f] National Laboratory of Astana, Nazarbayev University, Astana 010000, Kazakhstan

[g] School of Materials Science & Engineering; Tianjin Key Laboratory of Molecular Optoelectronic Sciences; Collaborative Innovation Center of Chemical Science and Engineering (Tianjin), Tianjin University, Tianjin 300350, China

[h] College of Chemistry, Nankai University, Tianjin, China

[i] State Key Laboratory of Supramolecular Structure and Materials, College of Chemistry, Jilin University, Changchun 130012, China

‡ X. Sun, F. Wang and G. Yang contributed equally to this work.

1. Device fabrication

OSCs device fabrication

The OSC devices were fabricated with the conventional configuration of glass/ITO/SAMs/active layer/C60/BCP/Ag. The patterned ITO-coated glass substrate (15 Ω/sq) was cleaned with detergent and deionized water ultrasonic cleaning 20 min, then continuously cleaned three times with acetone, and isopropanol for 15 min of each step. After that the substrate was dried with a nitrogen gun and then placed in an ultraviolet-ozone cleaning machine for 20 min. This step can further remove the organic residue on the substrate surface and improve the hydrophilicity of the substrate surface. The 4PADCB or 4PADCB+TCB (weight ratio of 1:1) were dissolved in isopropanol (IPA) with a concentration of 0.5 mg/mL and placed into an ultrasonic bath for 20 min. The SAM solution (65 μL for a 1.5 × 1.5 cm^2 substrate) was applied directly onto the ITO substrate for 40 s followed by a spin-coating step at 3000 rpm for 30 s. The ITO/SAM substrate was then placed onto a hotplate and annealed at 100 ℃ for 10 min. Finally, the ITO/SAM substrates were transferred inside a dry nitrogen glove box for solar cell fabrication. The PM6, BTP-eC9, Y6 and $PC_{71}BM$ were purchased from organtec.ltd. For the PM6: BTP-eC9 system, the PM6:BTP-eC9 solution was prepared by dissolving blends with a weight ratio of 1:1.2 in chloroform (total concentration 15.4 mg/mL) and stirred at room temperature for 2 hours. The active layer was spin-coated on the ITO/SAM substrates at 3500 rpm and then annealed 5 min at 80 ℃. Finally, C60 (10 nm)/BCP (5 nm)/Ag (100 nm)

layers were deposited to complete the device fabrication.

Wide-bandgap perovskite single-junction device fabrication

The substrates were then spin-coated with NiO_X (10 mg/mL in deionized water) nanoparticle dispersion. Then, the films were transferred to a nitrogen-filled glovebox and the Me-4PACz (1 mg/mL in IPA) was spin-coated on the substrates at 4,000 rpm for 30 s and heated at 100℃ for 10 min. The 1 M perovskite ($Cs_{0.25}FA_{0.75}Pb(Br_{0.5}I_{0.5})_3$) precursor solution used contains 129 mg FAI, 65 mg CsI, 275 mg $PbBr_2$, and 115 mg PbI_2, which were dissolved in 1 mL mixed solvent of DMF:DMSO (v/v = 4:1). Then, the precursor solution was shaken overnight at 60℃. For the spin-coating process, the substrate was spun at 4,000 rpm for 45 s with an acceleration of 4,000 rpm/s, and 200 mL of MeAc was slowly dropped at 15 s before the spin-coating ended. The perovskite

films were then annealed at 100℃ for 15 min. Then, the C60 (10 nm)/BCP (5 nm)/Ag (100 nm) layers were deposited to complete the device fabrication.

Perovskite-organic tandem device fabrication

After completing the deposition of the BCP layer, Ag (1 nm)/MoO_X (15 nm)was thermally evaporated on top of BCP and the film was brought back to the nitrogen-filled glovebox, then completed the deposition of the SAM layer. For the narrow band-gap PM6:BTP-eC9 system, the solution was prepared by dissolving blends with a weight ratio of 1:1:0.2 in chloroform (total concentration 15.4 mg/mL) and stirred at room temperature for 2 hours. The active layer was spin-coated on the ITO/SAM

substrates at 3500 rpm and then annealed 5 min at 80 ℃. Finally, C60 (10 nm)/BCP (5 nm)/Ag (100 nm) layers were deposited to complete the device fabrication.

2. Device performance characterization

The *J-V* characteristics were performed in N_2-filled glovebox under AM 1.5G (100 mW/cm^2) by using a Keithley 2400 source meter unit and an AAA solar simulator (SS-F5-3A, Enli Technology CO., Ltd.) calibrated by a standard Si photovoltaic cell. The external quantum efficiency (EQE) was measured by a certified incident photon to electron conversion (IPCE) equipment (QE-R) from Enli Technology Co., Lt. The light intensity at each wavelength was calibrated using a standard monocrystalline Si photovoltaic cell. The bias illumination obtained by applying a 500 nm short-pass filter, and an 800 nm long-pass filter was used for the measurements of the bottom subcell and the front subcell of perovskite-OPV TSC, respectively.

The analysis of J_{ph} *vs* V_{eff} relationships

The definition of J_{ph} is the current density under illumination (J_L) minus the dark current density (J_D), and V_0 refers to the voltage value when J_{ph} = 0. Accordingly, V_{eff} = V_0 - V_{appl}, where V_{appl} represents applied voltage, has a clear meaning. Importantly, when V_{eff} reaches a high value (> 2V) it is normally believed that generated excitons are fully collected, in which J_{ph} is equal to saturated current density (J_{sat}). Then, we can calculate J_{SC}/J_{sat} and J_{max}/J_{sat} to describe exciton dissociation (η_{diss}) and charge collection (η_{coll}) efficiency. J_{max} is the J_{ph} at the maximal output point.

Transient photovoltage (TPV) and transient photocurrent (TPC)

For TPV, the measurement was conducted under 1 sun conditions by illuminating the device with a white light-emitting diode, and the champion device is set to the open-circuit condition. For TPC, the champion device is set to the short-circuit condition in dark. The output signal was collected by key sight oscilloscope.

Electrochemical analysis

Mott-Schottky characteristics and Nyquist plots were conducted using a PARSTAT 4000A electrochemical workstation, employing a three-electrode setup. For the curve fitting of Mott-Schottky plots, the data were extracted by linear fitting the drop region of Mott-Schottky plots, and V_{bi} was obtained via the intercept of the straight line with the X axis.

Hole Mobility Measurements

The mobilities were measured by using a space charge limited current (SCLC) model with the hole-only device of glass/ITO/SAMs/PM6: BTP-eC9/MoO3/Ag. Hole mobility was obtained by fitting the current density-voltage curves and calculated by the equation[1]:

$$J(V) = \frac{9}{8}\varepsilon_0\varepsilon_r\mu\frac{V^2}{L^2}\#(1)$$

Where J is current density, ε_0 is the permittivity of free space (8.85×10^{-14} F/cm), ε_r is the relative permittivity of the material (assumed to 3), μ is hole mobility or electron mobility, V is applied voltage and L is the thickness of film (~110 nm).

EQE_{EL} measurements

EQEEL measurements were done using a home-built setup using a Keithley 2400 to

inject current to the solar cells. Emission photon-flux from the solar cells was recorded using a Si detector (Hamamatsu s1337-1010BQ) and a Keithley 6482 picoammeter.

Urbach energy (E_U)

E_U can be calculated from the slope of the straight line by plotting ln (α) against the incident photon energy (E), which follows the straight-line equation below:

$$\ln \alpha(E) = \ln \alpha_0 + \frac{E}{E_u} - \frac{E_g}{E_u} \#(2)\#$$

3. Characterization of SAM

Instruments and characterization

Nuclear magnetic resonance (NMR) spectroscopy

1H NMR and 31P NMR spectra were recorded on Bruker (AVANCE III 400MHz). X-ray photoelectron spectroscopy (XPS) was measured by Thermo Scientific K-Alpha.

Contact angle measurements

The contact angles of water and formamide (FA) on SAMs coated ITO were measured by a video optical contact angle meter (DSA-100 (KRUSS Germany)). Then the surface free energy was calculated by Owens-Wendt method:[2, 3]

$$\gamma_L \times (1 + cos\theta) = 2 \times \left(\gamma_L^d \cdot \gamma_{sv}^d\right)^{\frac{1}{2}} + 2 \times \left(\gamma_L^p \cdot \gamma_{sv}^p\right)^{\frac{1}{2}} \#(3)$$

where γ_L and γ_{sv} are surface free energy of the probe liquid and sample, respectively. The θ is the contact γ_L angle of the sample. The Flory-Huggins interaction parameter

$\chi_{\text{donor-acceptor}}$ for blends to show the binary miscibility was calculated from the equation:

$$\chi_{door-acceptor} = K\left(\gamma_{donor}^{\frac{1}{2}} - \gamma_{donor}^{\frac{1}{2}}\right)^2 \#(4)$$

where γ is the surface energy of the material, *K* is the proportionality constant.

GIWAXS and XRD Measurement

GIWAXS measurements were performed at the Synchrotron & Printable Electronic Lab, Hoffmann Institute of Advanced Materials, Shenzhen Polytechnic University with SAXSFocus 3.0 (GKINST Co., LTD.) equipped with a Cu X-ray Source (8.05 keV, 1.54 Å) and an EIGER 2R 500K detector. The incident angle during the measurement was maintained at 0.5° and the distance between sample and detector was 132 mm.

For the GIWAXS and XRD measurement of SAM layers, the films were prepared by spin-coating the control and TCB-treated SAM precursor solutions (2 mg/mL in IPA) at 500 rpm for 30 s, followed by annealing at 130 °C for 5 min, the thicker films are beneficial to obtain better signals.

Theoretical calculations

All the calculations of the model compounds studied in this work were performed using the Gaussian 09 software package. Ground state geometry optimizations of 4PADCB, and TCB are calculated by DFT at the B3LYP/6-31G (d, p) (empirical dispersion = gd3bj) level. The visualization of the molecular orbitals and ESP distribution was performed using GaussView 6.0.16 and VMD software.[4] The

reduced density gradient analysis was performed using MultiWfn3.8 software.[5, 6]

4. Characterization of the active layer

Film-depth-dependent light absorption and composition distribution

Film-depth-dependent light absorption was carried out with an in-situ spectrometer (PU100, Shaanxi Puguang Weishi Co. Ltd.) equipped with a soft plasma-ion source. A 100 W power with an input pressure of ~10 Pa (oxygen) was used to generate soft ionic source. The surface of the target film is gradually etched by the soft ion source, without damage to the materials underneath. The absorption for the film during etching was in-situ monitored by a spectrometer.

Atomic Force Microscopy (AFM) measurements

Topographic images of the films were obtained from a Bruker atomic force microscopy (AFM) with the type of dimension edge with Scan Asyst in the tapping mode using an etched silicon cantilever at a nominal load of ~2 nN, the scanning rate for a 1 μm×1 μm image size was 0.9 Hz and 5 μm×5 μm image size was 1.0 Hz.

HAADF-TEM measurements

The films were floated off the substrates in deionized water and collected on lacey carbon coated TEM grids (Electron Microscopy Sciences). HAADF-TEM were performed on a Thermo Fischer Talos-200S TEM equipped with an electron monochromator and a Gatan Imaging Filter (GIF) Quantum 966.

GIWAXS and GISAXS Measurement

The samples were fabricated by spin-coating the active layer precursor solutions onto

Si substrates. The incidence angles are 0.12° and the distances between sample and detector are 132 mm (GIWAXS) and 1000 mm (GISAXS) respectively. One dimensional experimental data were obtained with the SGTools software package programmed by Zhao et al.[7]

Data analysis.

The ordering degree of SAMs was quantified by using the Herman's orientation factor (*f*), which is defined as follows:

$$f = \frac{1}{2}(3\langle cos^2\theta\rangle - 1) \#(5)$$

where the $\langle cos^2\theta\rangle$ is the average value of the square of the cosine of the azimuthal angle for the scattering peak, which is calculated as follows:

$$\langle cos^2\theta\rangle = \frac{\int_{min}^{\pi/2} I(\theta) cos^2(\theta) \sin(\theta) d\theta}{\int_{min}^{\pi/2} I(\theta) \sin(\theta) d\theta} \#(6)$$

where $I(\theta)$ is the intensity at an azimuthal angle of θ.

The structural information of blend films such as the period of arrangement and lamellar stacking spacing is obtained via the Bragg equation, as well as the crystal coherence length (*CCL*) can be obtained from the Scherrer formula,[8] and the specific expressions of the Bragg equation and Scherrer formula are as follows:

$$d = \frac{\lambda}{2\sin(\theta)} = \frac{2\pi}{q} \#(7)$$

$$CCL = \frac{K\lambda}{FWHM \cdot \cos(\theta)} \#(8)$$

where d is the lamellar stacking spacing, and CCL is the crystal domain along the specified direction called crystal coherence length, which is generally considered to be equivalent to the grain size. λ is the value of X-ray wavelength; K is a dimensionless shape factor,[9] generally taken as K = 0.89; FWHM is the half-peak width of the scattering peak; θ is the scattering angle.

GISAXS fitting model

To quantify and compare the phase separation, the IP (in plane) scattering profiles are fitted with a model that describes the scattering contribution of each phase, the fitting equation is shown in Eq. (1):

$$I(q) = \frac{A_1}{\left[1 + (q\xi)^2\right]^2} + A_2\langle P(q,R)\rangle S(q,R,\eta,D) + B \#(9)$$

where the first term was the so-called Debye-Anderson-Brumberger (DAB) term[10], modeling the scattering from the amorphous intermixing domains, and ξ is the average correlation length of the amorphous domain.

The second term is the scattering intensity contribution from the small molecule pure domains in the co-monomer, where $P(q,\ R)$ is the shape factor of the pure domains. $S(q,\ R,\ \eta,\ D)$ is the structure factor of pure domains, and the fractal-like network model is generally used to describe the cluster domains in the films expressed as follows:

$$S(q) = 1 + \frac{\sin\left[(D-1)\tan^{-1}(q\eta)\right]}{(qR)^D} \cdot \frac{D\Gamma(D-1)}{\left[1 + \frac{1}{(q\eta)^2}\right]^{\frac{(D-1)}{2}}} \#(10)$$

where R is the mean radius, η is the coherence length of the fractal network, and D is the fractal dimension of the structure. The average domain size can be estimated by

the Guinier radius of the fractal-like network *Rg* expressed as follows:

$$R_g = \left[\frac{D(D+1)}{2}\right]^{\frac{1}{2}}\eta \#(11)$$

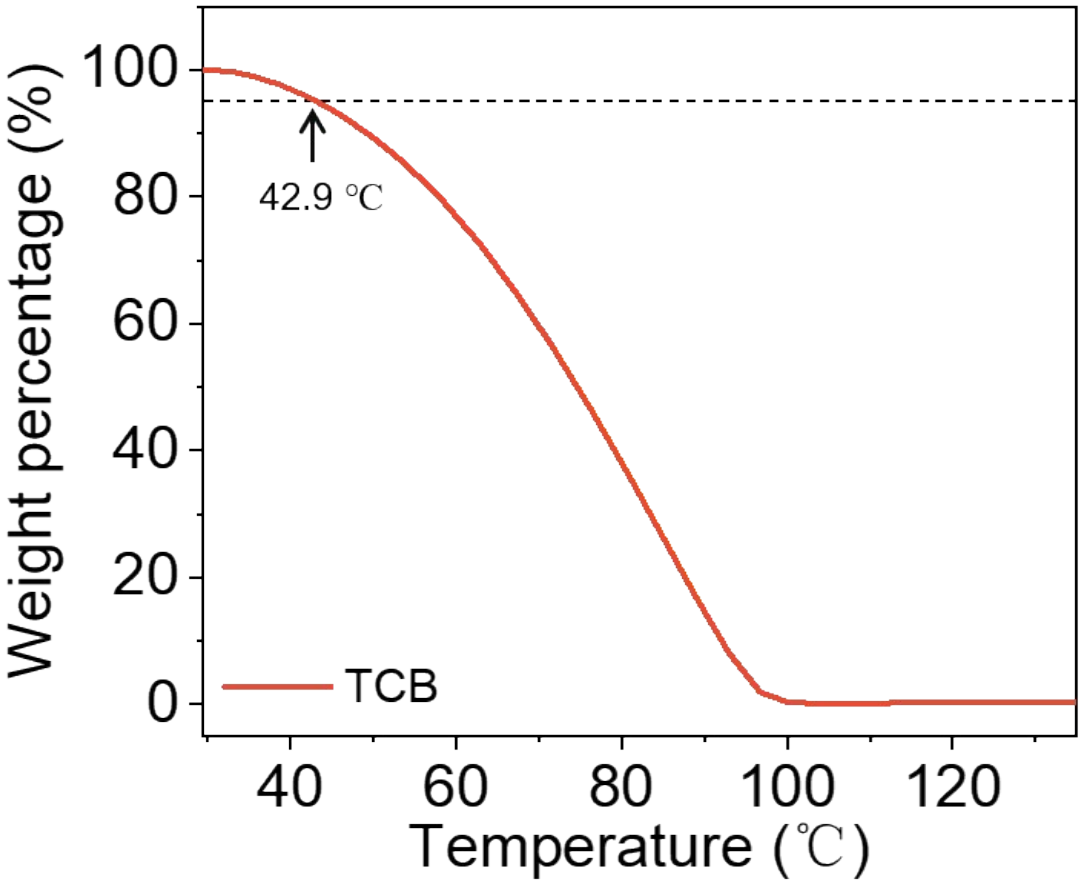

Fig. S1 TGA plots of TCB at a scan rate of 10°C min^{-1} under inert atmosphere.

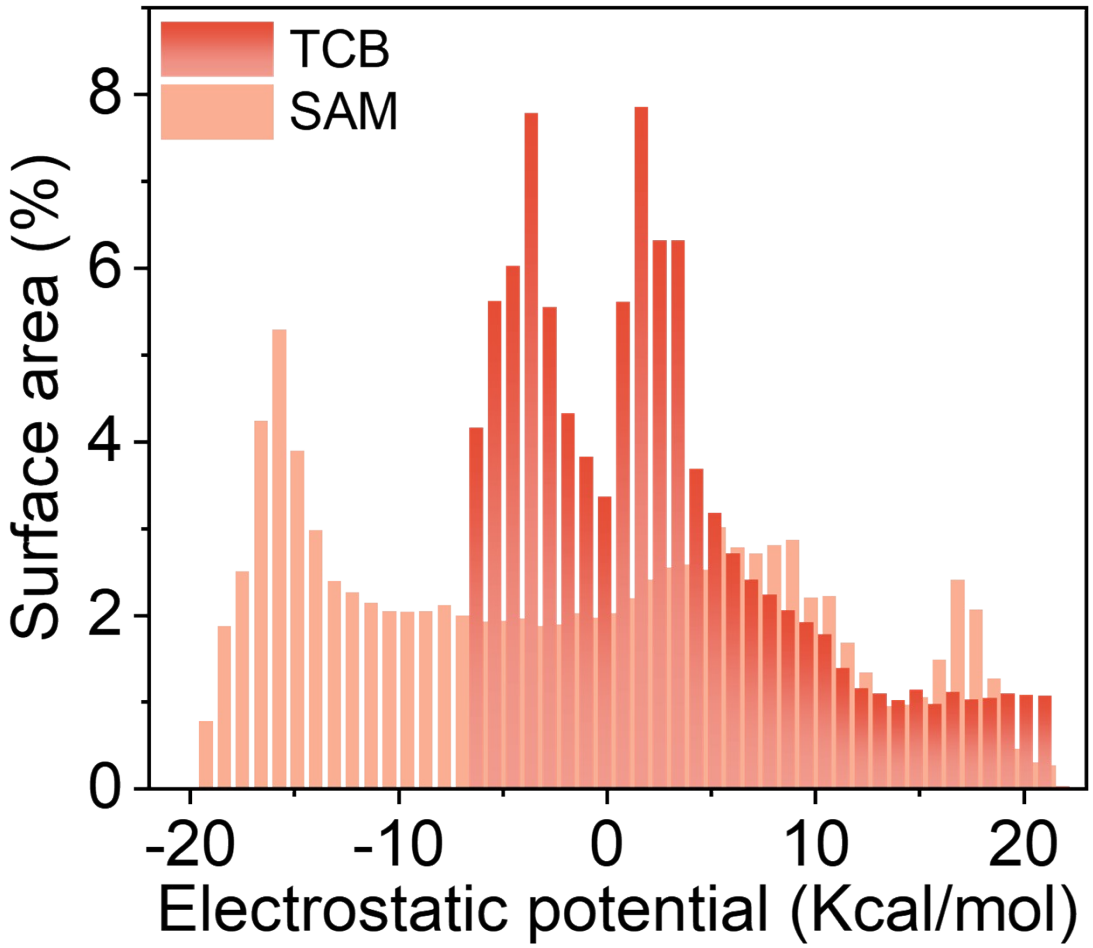

Fig. S2 Quantitative analysis of the histograms of electrostatic potential area distribution of TCB and SAM.

Table S1 The the overall average ESP values of DCB core and TCB, respectively.

	Overall average value (kcal/mol)
DCB Core	-1.11
TCB	2.33

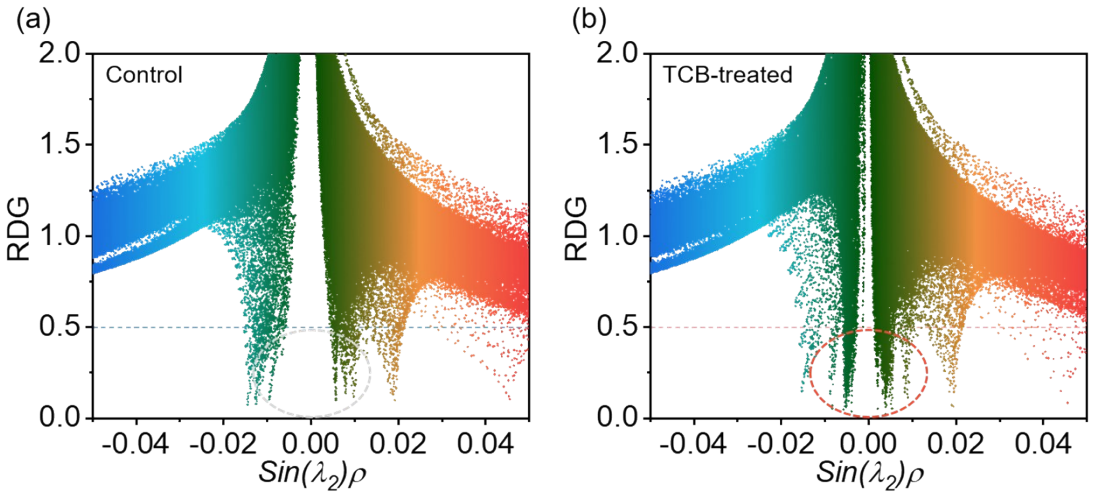

Fig. S3 The functions of RDG and Sign $(\lambda_2)\rho$ for (a) control and (b) TCB-treated SAM.

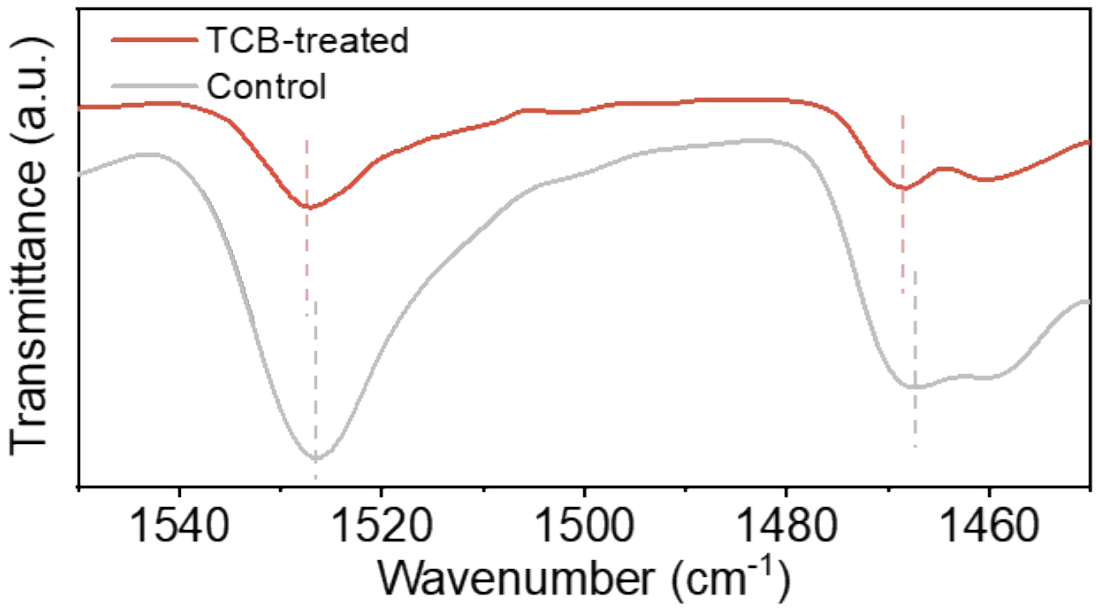

Fig. S4 The FTIR spectra of control and TCB-treated SAM.

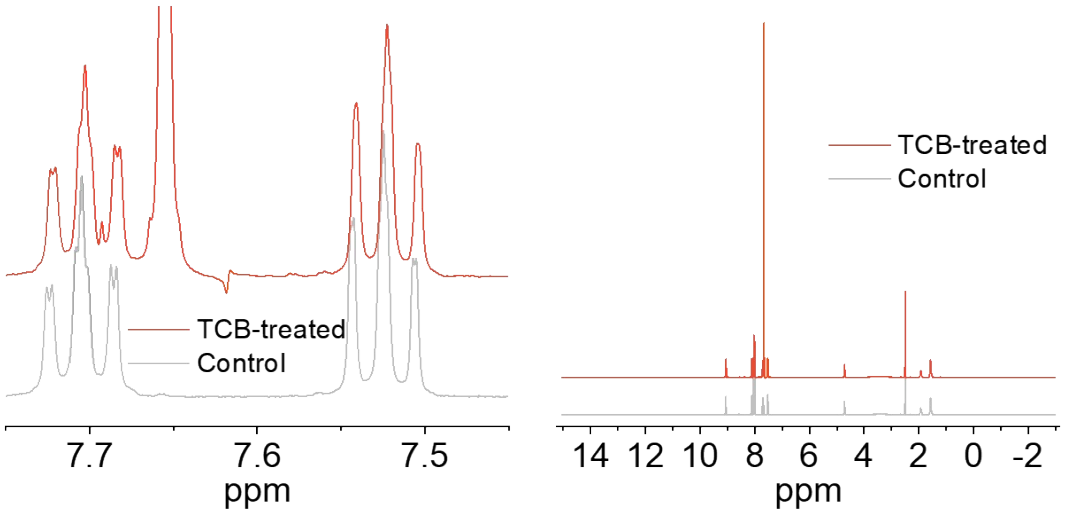

Fig. S5 ^{1}H NMR spectra of control and TCB-treated SAM.

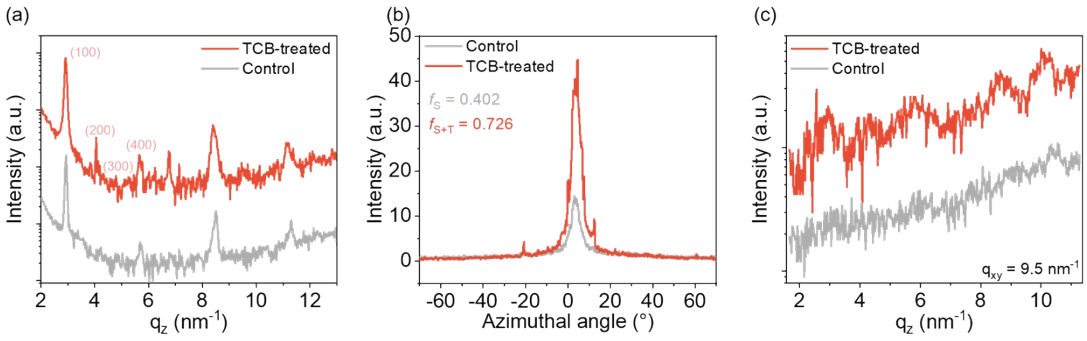

Fig. S6 The scattering profile of SAMs on (a) OOP direction, (b) azimulth degree and (c) $q_{xy} \approx 9.5 nm^{-1}$.

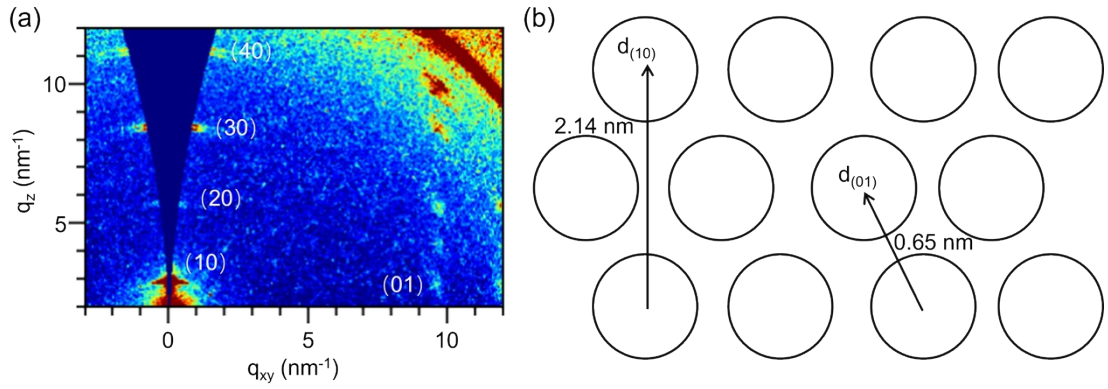

Fig. S7 (a) 2D GIWAXS patterns of TCB-treated SAM layer. (b) Representation of the 2D hex and rectangular unit.

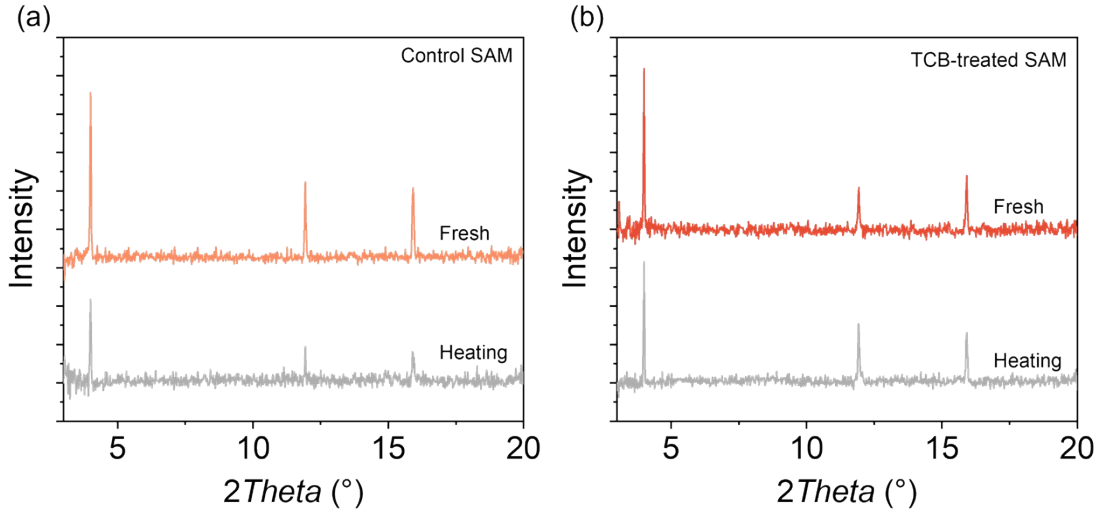

Fig. S8 (a)(b) XRD patterns of control and TCB-treated SAM layer before and after ageing tests of thermal annealing

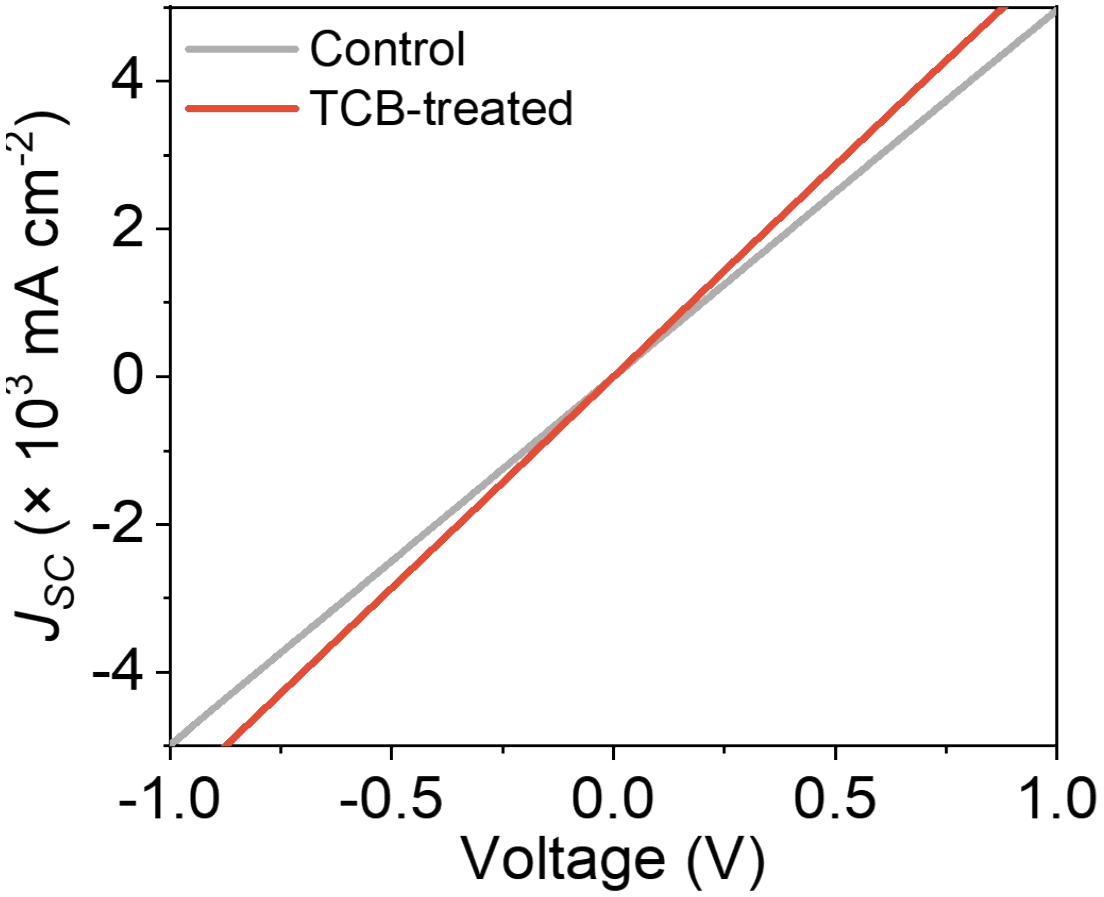

Fig. S9 (a) *J-V* dark curves of the device with the structure of ITO/control and TCB-treated SAM/Ag.

Table S2 Detailed device parameters with varied concentration of TCB.

TCB Concentration (mg/mL)	***V*$_{OC}$ (V)**	***J*$_{SC}$ (mA cm^{-2})**	***FF***	**PCE (%)**
0.1	0.860	28.38	79.63	19.44
0.3	0.862	28.57	79.41	19.54
0.5	0.863	28.83	80.64	20.06
0.8	0.863	28.57	79.74	19.67
1.0	0.863	28.45	79.69	19.57

Table S3 Detailed device parameters with varied TA temperatures of SAM layer.

Temperature (℃)	V_{OC} (V)	J_{SC} (mA cm-2)	FF	PCE (%)
80	0.863	28.64	78.94	19.52
100	0.863	28.83	80.64	20.06
120	0.864	28.79	78.85	19.62

华南国家计量测试中心
广东省计量科学研究院
SOUTH CHINA NATIONAL CENTER OF METROLOGY
GUANGDONG INSTITUTE OF METROLOGY

校 准 证 书
CALIBRATION CERTIFICATE

证书编号 Certificate No. NYX202400562 第 1 页，共 5 页 Page of

客户名称 Name of the Customer 深圳职业技术大学霍夫曼先进材料研究院 Hoffmann Institute of Advanced Materials,Shenzhen Polytechnic University
联络信息 Contact Information 广东省深圳市南山区留仙大道7098号 No.7098 Liuxian Avenue,Nanshan District,Shenzhen City,Guangdong Province
计量器具名称 Description 非富勒烯有机太阳能电池 Non-fullerene organic solar cells
型号/规格 Model/Type 非富勒烯有机太阳能电池 Non-fullerene organic solar cells
制造厂 Manufacturer 深圳职业技术大学霍夫曼先进材料研究院 Hoffmann Institute of Advanced Materials,Shenzhen Polytechnic University
出厂编号 Serial No. SX-6 设备管理编号 Equipment No. ----
接收日期 Receipt on 2024 年 12 月 25 日 Y M D
结论 Conclusion 见校准结果 Shown in the results of calibration
校准日期 Calibration on 2024 年 12 月 25 日 Y M D
发布日期 Issue on 2025 年 01 月 03 日 Y M D

批 准 Authorized by 吴江宏
核 验 Reviewed by 易国贤
校 准 Calibrated by 梅书刚

华南国家计量测试中心 证书专用章

扫一扫查真伪

实验室地址：广东省东莞市石排镇东园大道石排段152号 邮政编码：523343
电话：(8620) 86594172 传真：(8620) 86590743 投诉电话：(8620)30611242 E-mail：scm@scm.com.cn
Add: No.1 Miaobianwang Section, Dongyuan Road South, Shipai Town, Dongguan, Guangdong.
Post Code: 523343 Tel: (8620)86594172 Fax: (8620)86590743 Complaint Tel: (8620)30611242
证书真伪查询：www.scm.com.cn; cert.scm.com.cn Certificate Authenticity Identify: www.scm.com.cn; cert.scm.com.cn

5241226001 2

华南国家计量测试中心
广东省计量科学研究院
SOUTH CHINA NATIONAL CENTER OF METROLOGY
GUANGDONG INSTITUTE OF METROLOGY

说　明

证书编号　NYX202400562
Certificate No.

DIRECTIONS

第 2 页，共 5 页
Page of

1. 本中心是国家市场监督管理总局在华南地区设立的国家法定计量检定机构，本中心的质量管理体系符合ISO/IEC 17025:2017标准的要求。
This laboratory is the National Legal Metrological Verification Institution in southern China set up by the State Administration for Market Regulation. The quality system is in accordance with ISO/IEC 17025:2017.

2. 本中心所出具的数据均可溯源至国家计量基准和/或国际单位制(SI)。
All data issued by this laboratory are traceable to national primary standards and/or International System of Units (SI).

3. 校准地点、环境条件：
Location and environmental conditions of the calibration:
地点　本院二基地A1-402　　温度　(25±2) ℃　相对湿度　(30±5) %
Place　Temperature　R.H.

4. 本次校准的技术依据：
Reference documents for the calibration:
JJF1622-2017 太阳电池校准规范：光电性能　C.S. for Solar Cells: Photoelectric Properties

5. 本次校准所使用的主要计量标准器具：
Major standards of measurement used in the calibration:

设备名称/型号规格/测量范围 Name of Equipment /Model/Type/Range	编号 Serial No.	证书号/有效期/溯源单位 Certificate No./Due Date /Traceability to	计量特性 Metrological Characteristic
ABET 稳态太阳模拟器 1000W full spectrum solar simulator /SUN3000/(300~1300)W/m²	374	NYX202400537 /2025-12-03 /本中心	光谱匹配度：A级 辐照度不均匀性：A级 辐照度不稳性：A级
标准太阳能电池 Standard Solar Cell /RR_257_0/　Isc：(1~200)m A	13/01/2014	GXgf2024-06295 /2025-09-24 /中国计量院	U_{rel}=2.2%，k=2
标准源表 Standard Source Meter /2420/(0~60)V, (0~3)A	4051271	DB2024034O1 /2025-02-26 /本中心	电压：U_{rel}=0.1%，电流：U_{rel}=0.1%(k=2) DCV：U_{rel}=0.1%，DCA：U_{rel}=0.1%(k=2)

— 本说明页以下空白 —

注：1. 本证书校准结果只与受校准仪器有关。The results relate only to the items calibrated.
Note: 2. 未经本机构书面批准，不得部分复制此证书。This certificate shall not be reproduced except in full, without the written approval of our laboratory.
3. "客户名称"、"联络信息"由委托方提供，"制造厂"、"型号规格"、"出厂编号"以及"设备编号"为仪器上标注。委托方对上面内容如有异议，须在收到证书后二十个工作日内提出。
The information Name of the Customer and Contact Information are provided by client, and the Manufacturer, Model/Type, Serial No. and Equipment No. are marked on the items. Client shall submit any objection within 20 working days after receiving the certificate for the information above.

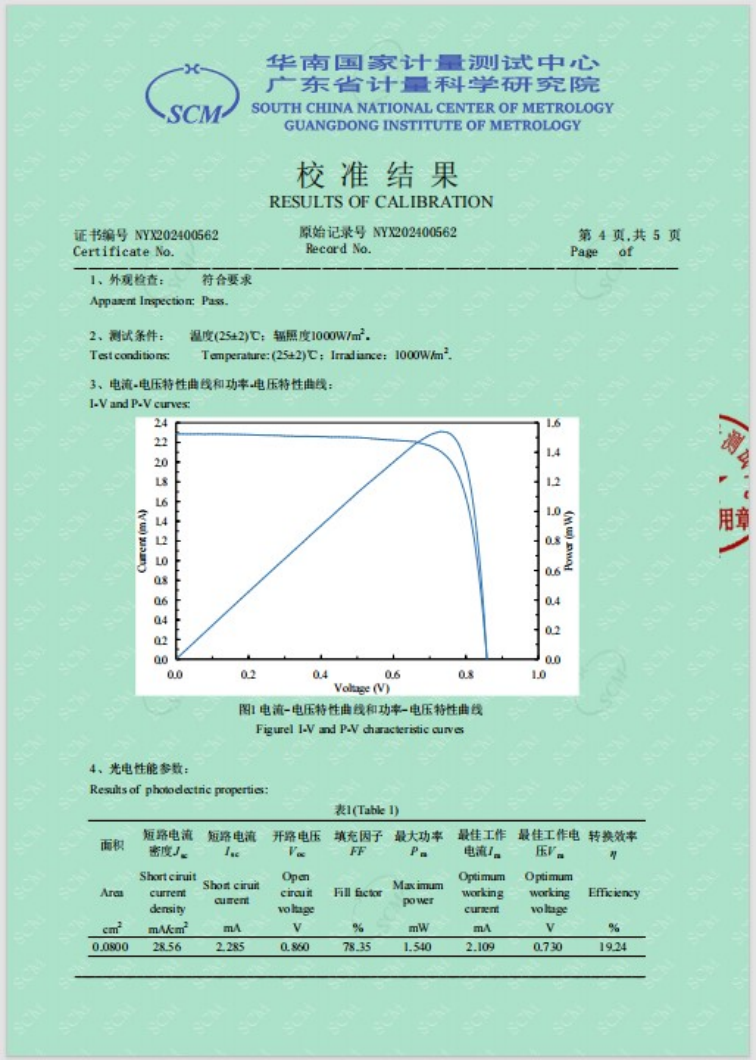

华南国家计量测试中心
广东省计量科学研究院
SOUTH CHINA NATIONAL CENTER OF METROLOGY
GUANGDONG INSTITUTE OF METROLOGY

校 准 结 果
RESULTS OF CALIBRATION

证书编号 NYX202400562 Certificate No.　原始记录号 NYX202400562 Record No.　第 4 页,共 5 页 Page of

1、外观检查： 符合要求
Appaent Inspection: Pass.

2、测试条件： 温度(25±2)℃；辐照度1000W/m².
Test conditions: Temperature: (25±2)℃; Irradiance: 1000W/m².

3、电流-电压特性曲线和功率-电压特性曲线：
I-V and P-V curves:

图1 电流-电压特性曲线和功率-电压特性曲线
Figurel I-V and P-V characteristic curves

4、光电性能参数：
Results of photoelectric properties:

表1(Table 1)

面积 Area	短路电流密度 J_{sc} Short circuit current density	短路电流 I_{sc} Short circuit current	开路电压 V_{oc} Open circuit voltage	填充因子 FF Fill factor	最大功率 P_m Maximum power	最佳工作电流 I_m Optimum working current	最佳工作电压 V_m Optimum working voltage	转换效率 η Efficiency
cm^2	mA/cm^2	mA	V	%	mW	mA	V	%
0.0800	28.56	2.285	0.860	78.35	1.540	2.109	0.730	19.24

Fig. S10 Certified Efficiency of PM6:BTP-eC9 binary OSCs device based on TCB-treated SAM.

Table S4 Summary of the photovoltaic parameter of the device based on control and TCB-treated SAM.

Active layers	Conditions	V_{OC} (V)	J_{SC} (mA cm^{-2})	*FF*	PCE(Average) (%)
PM6:BTP-eC9	Control	0.859	28.43	79.25	19.35
	Target	0.863	28.83	80.64	20.06
PM6:L8-BO	Control	0.910	26.68	78.91	19.16
	Target	0.909	25.88	78.72	18.51
PM6:Y6	Control	0.835	27.19	75.67	17.18
	Target	0.845	27.67	76.40	17.83
PM6:Y6:$PC_{71}BM$	Control	0.843	27.21	76.79	17.62
	Target	0.853	27.22	77.72	18.04

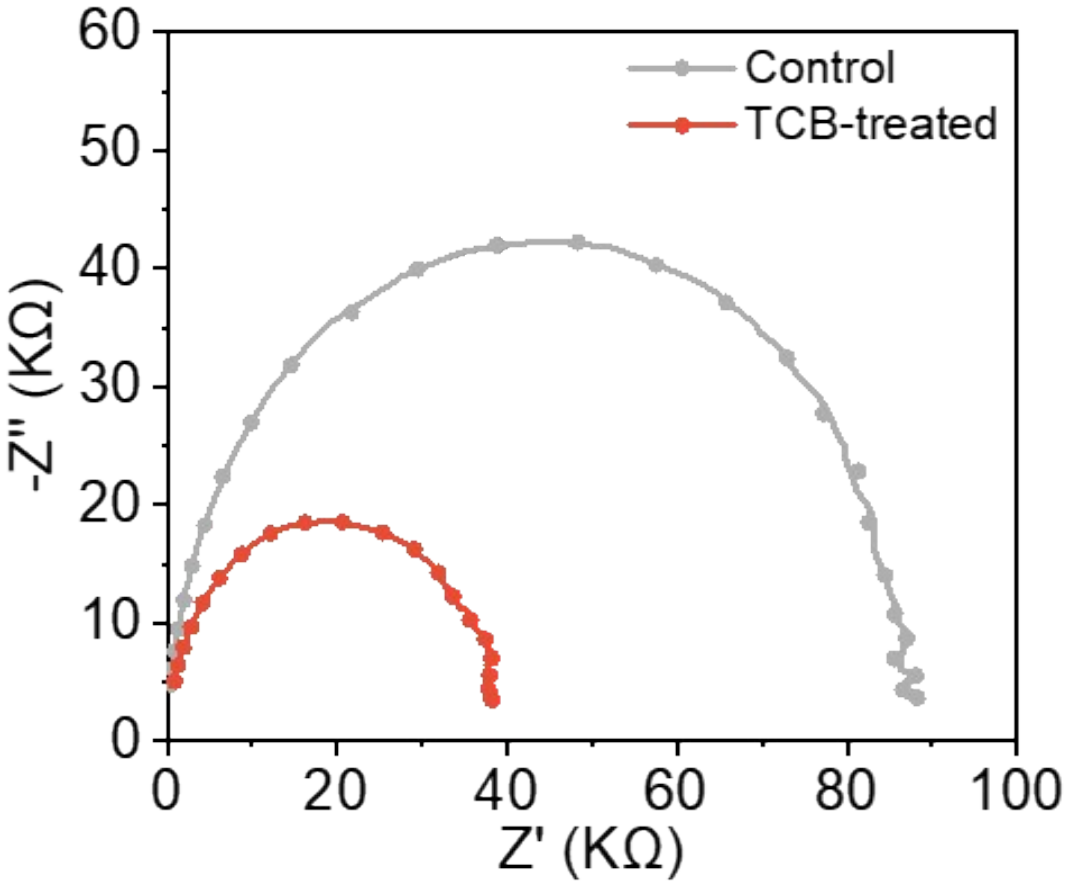

Fig. S11 Nyquist plots of devices based on control and TCB-treated SAM layer.

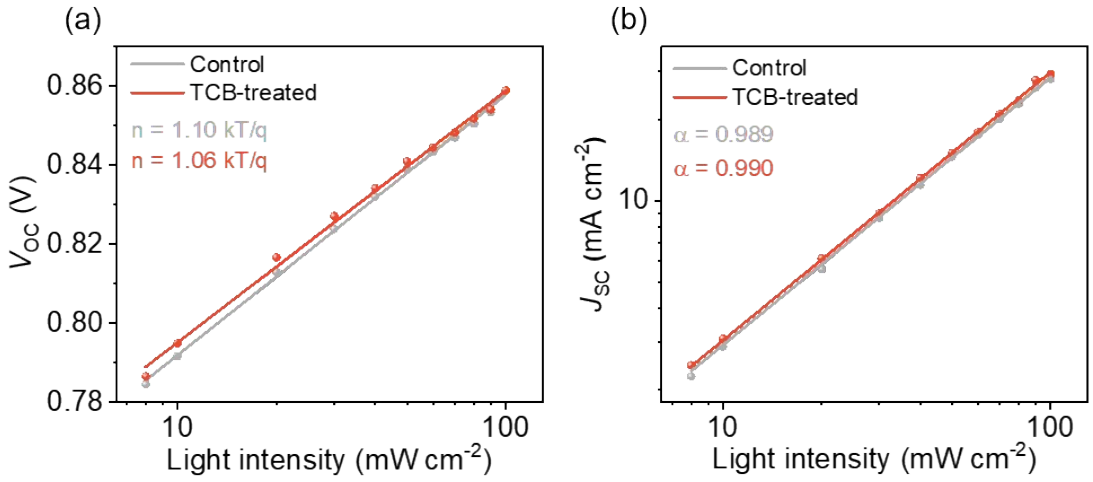

Fig. S12 V_{OC} and J_{SC} with different light intensity.

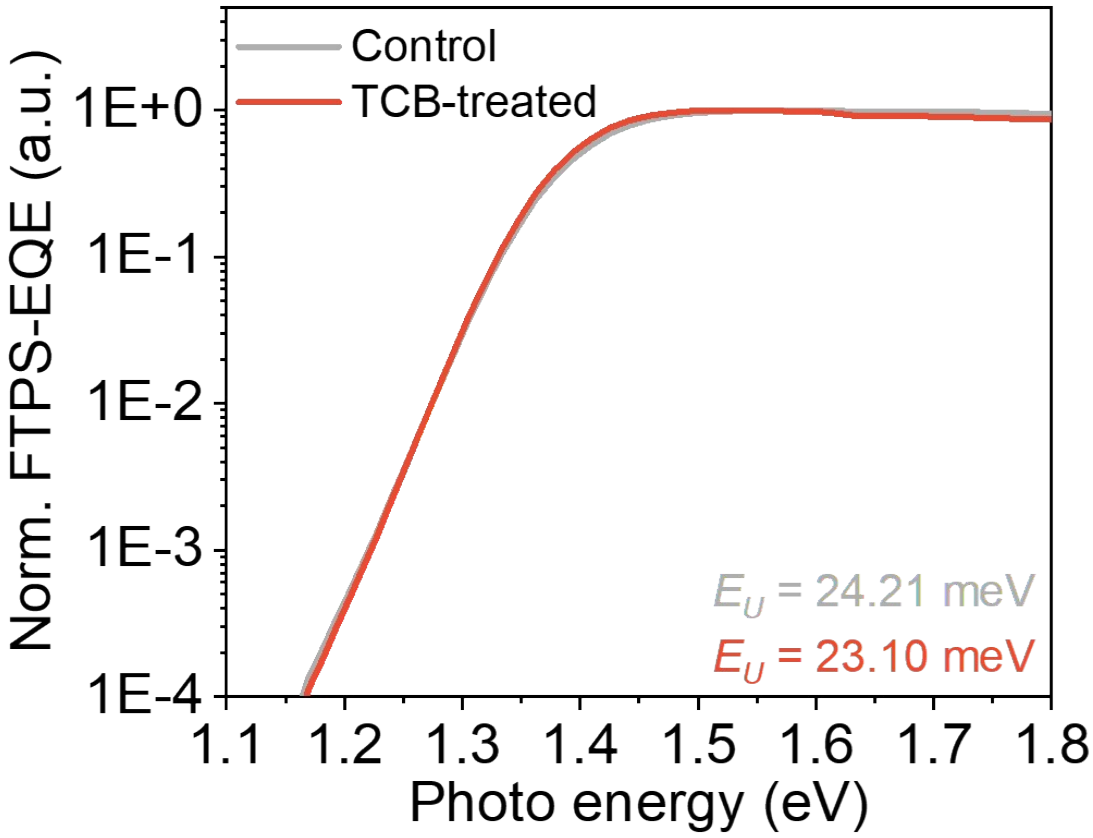

Fig. S13 FTPS-EQEs of the device based on control and TCB-treated SAM layer.

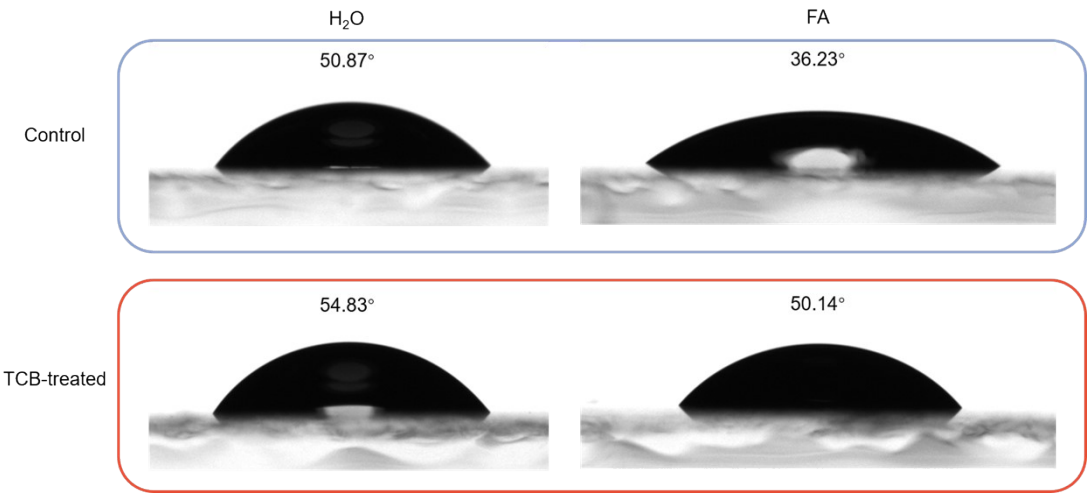

Fig. S14 Photographs of water and formamide droplets in contact with control and TCB-treated SAM layer.

Table S5 Surface energy (γ_s) of control and TCB-treated SAM layers.

HTL	Contact angle (°)		γ_s (mN m^{-1})
	H_2O	FA	
SAM	50.87	36.23	49.47
SAM+TCB	54.83	50.14	45.12

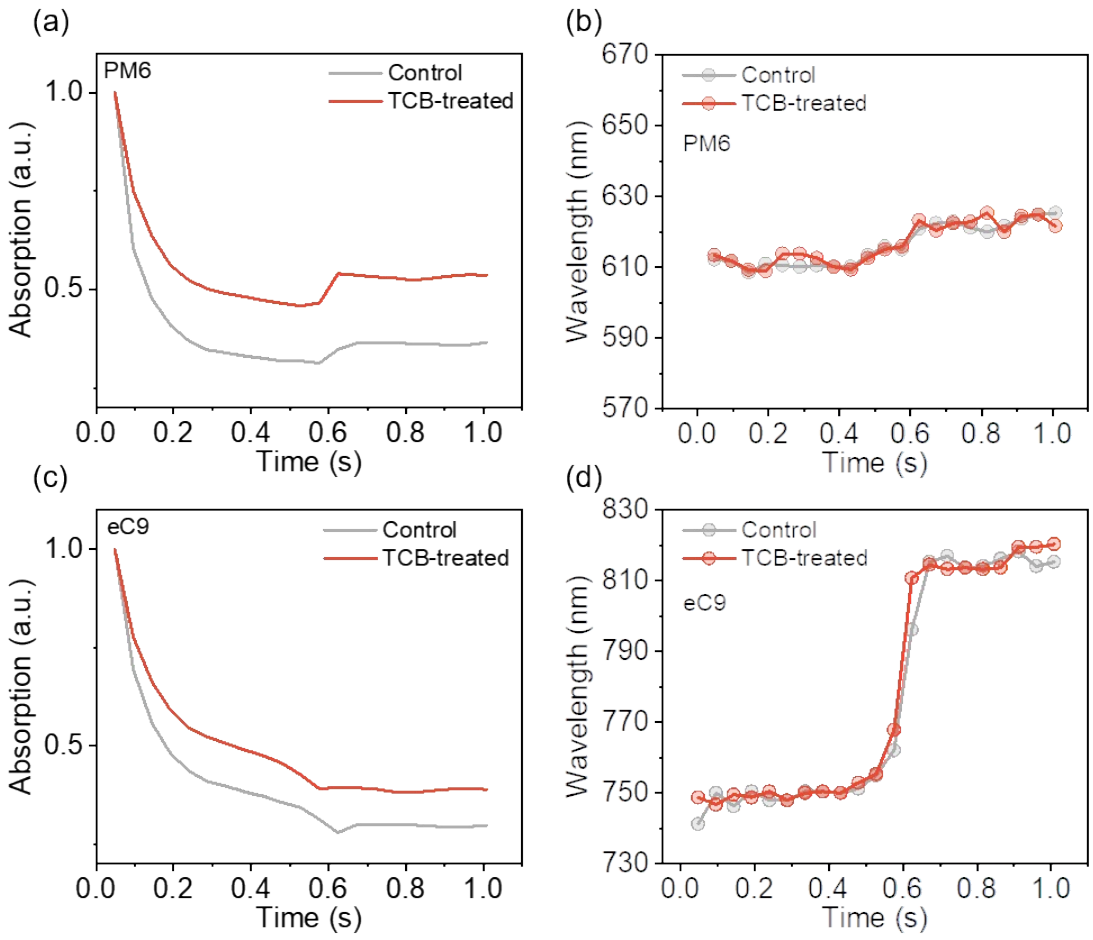

Fig. S15 The time evolutions of absorption peak of blend films during spin-coating.

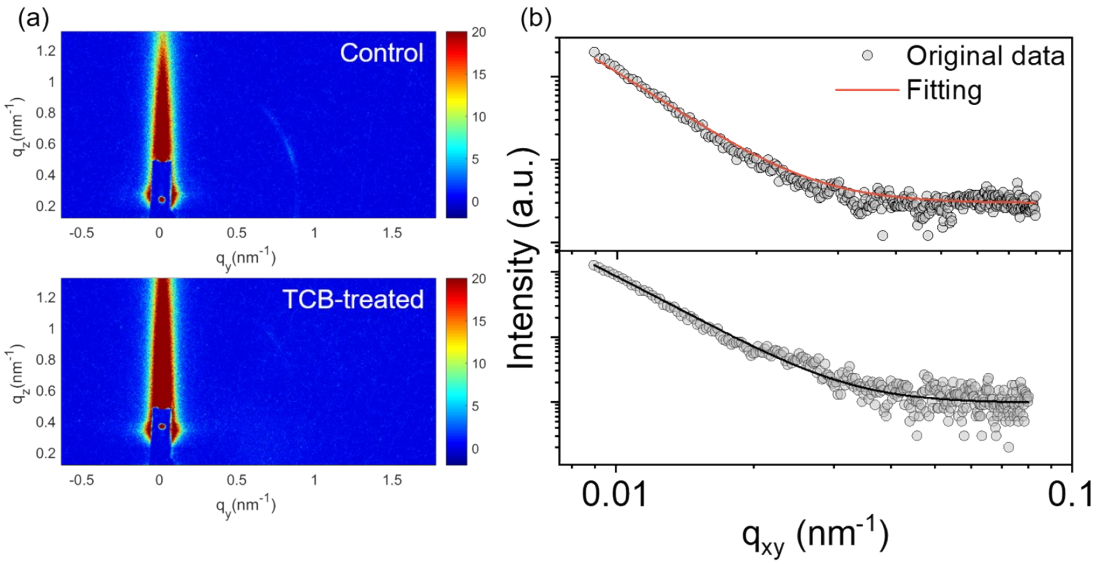

Fig. S16 (a) GISAXS patterns and (b) scattering profiles of Yoneda peaks.

Table S6 Fitting data obtained from GISAXS patterns.

Conditions	ξ (nm)	D	η (nm)	*Rg* (nm)
Control	30.3	1.9	9.4	15.6
TCB-treated	29.0	2.1	9.5	17.8

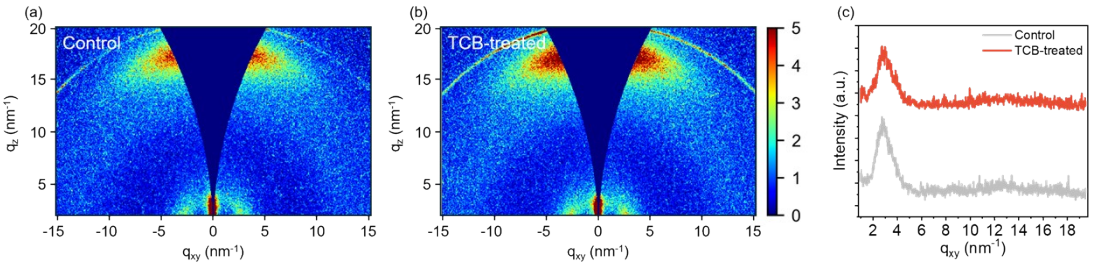

Fig. S17 GIWAXS patterns and scattering profiles of active layer based on (a) control and (b) TCB-treated SAM layer.

Table S7 Detailed (010) peak information in the OOP direction of active layer based on control and TCB-treated SAM layer.

Conditions	peak position (nm^{-1})	FWHM (nm^{-1})	*d*-spacing (nm)	*CCL* (nm)
Control	17.38	2.057	0.362	5.47
TCB-treated	17.45	2.001	0.360	5.62

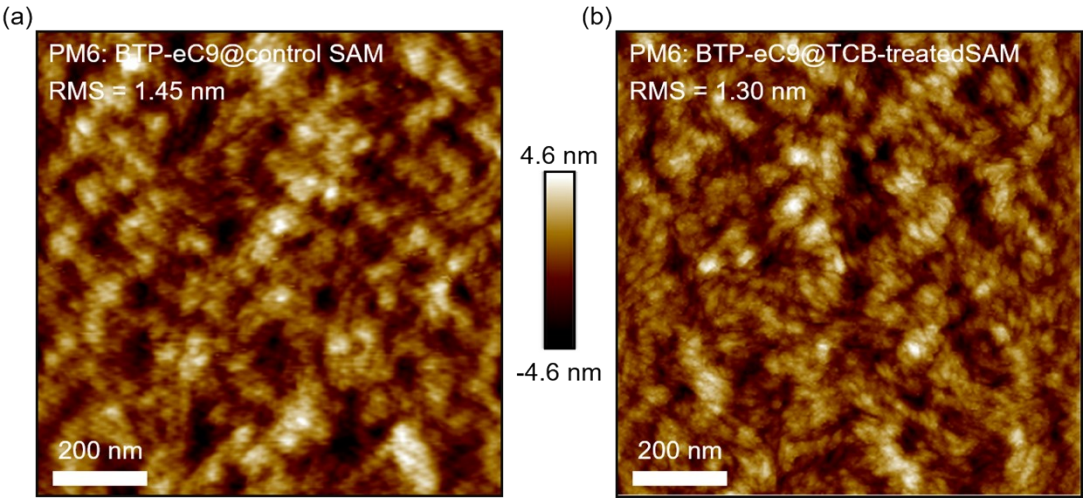

Fig. S18 AFM height images of active layer on (a) control and (b) TCB-treated SAM layer.

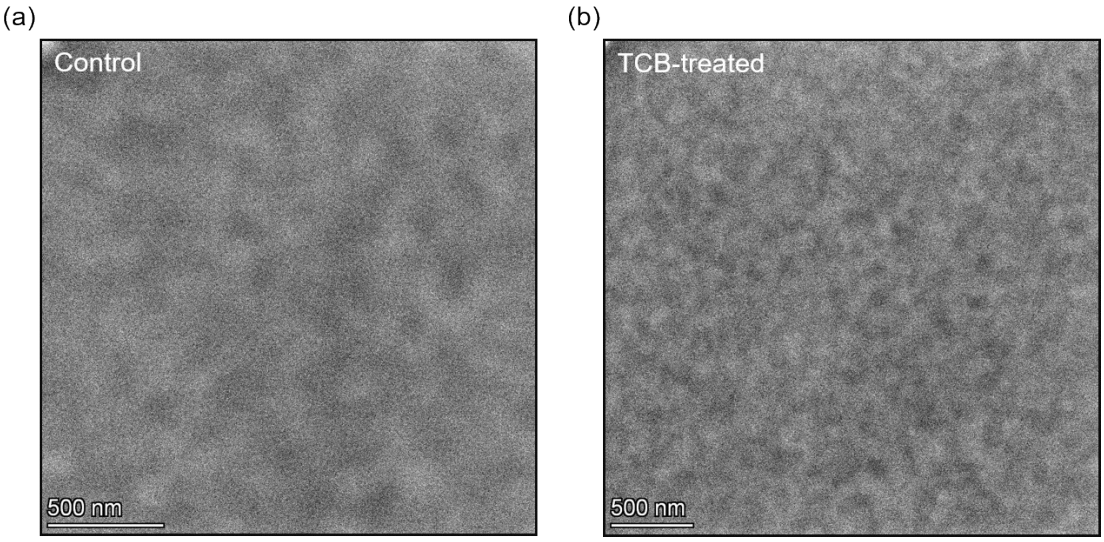

Fig. S19 TEM images of active layer on on (a) control and (b) TCB-treated SAM layer.

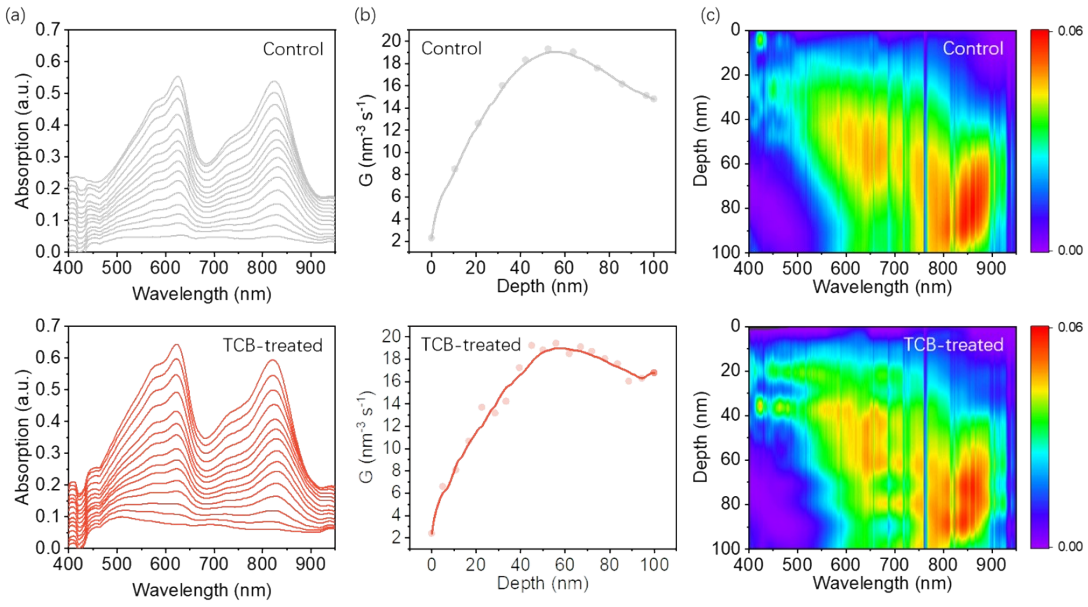

Fig. S20 (a) Film-depth-dependent absorption spectra, (b) exciton generation rate and c) contours of active layer on control and TCB-treated SAM layers.

Table S8. The photovaltaic patameters of single junction and tandem devices.

Band gap	V_{OC} (V)	J_{SC} (mA cm^{-2})	*FF*	PCE (%)
1.85eV PSCs	1.300	15.97	82.98	17.24
1.36eV OSCs	0.858	28.90	79.68	19.75
Tandem	2.131	14.95	81.90	26.09

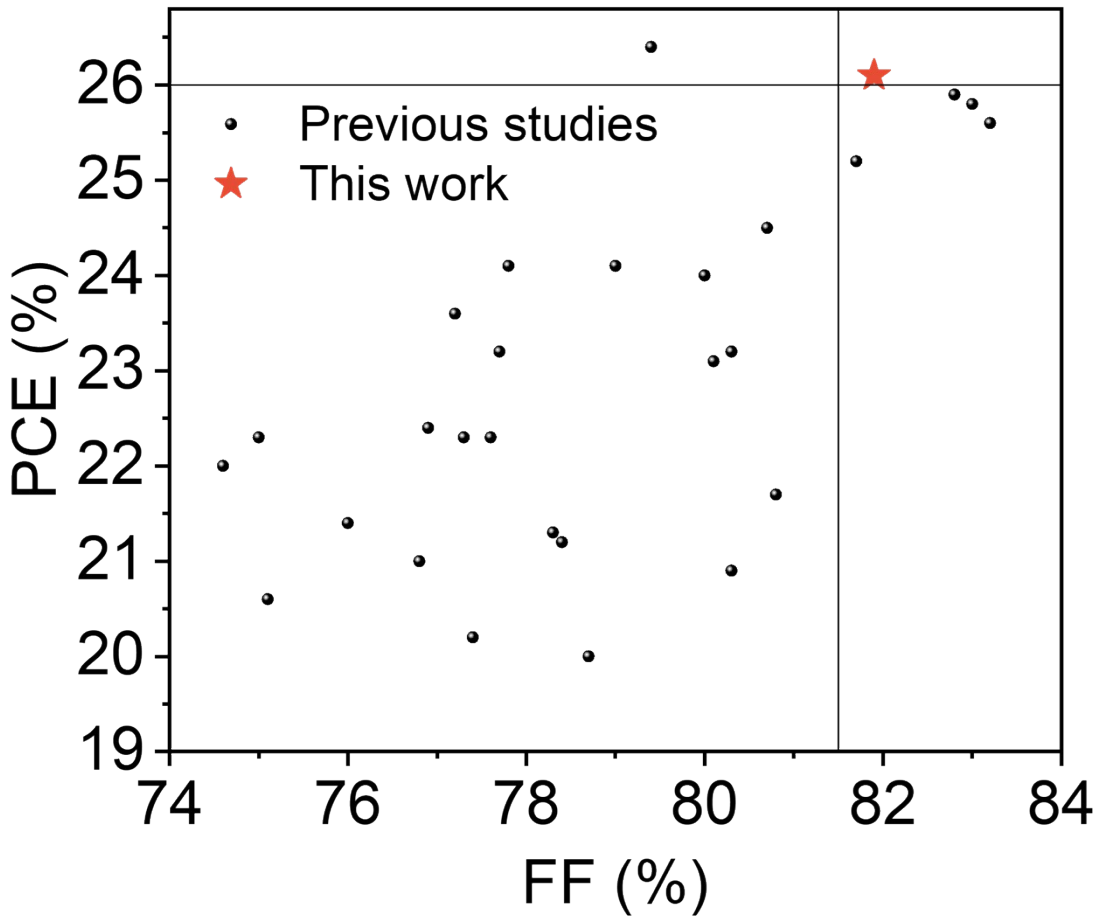

Fig. S21 Statistical PCE versus FF of perovskite/organic solar cells in this work and

results reported in the literature.

Table S9 Summary of photovoltaic performance of perovskite/organic solar cells in the literature.

V_{OC} (V)	J_{SC} (mA cm^{-2})	FF (%)	PCE (%)	*Ref.*
1.96	13.3	80.3	20.9	[11]
2.05	13.4	76.8	21.0	[12]
1.88	15.7	74.6	22.0	[13]
2.06	14.8	77.2	23.6 (22.9 certified)	[14]
1.96	13.8	78.4	21.2	[15]
2.15	14.0	80.0	24.0 (23.1 certified)	[16]
2.10	13.1	75.1	20.6	[17]
1.94	13.1	78.7	20.0	[18]
2.22	12.7	76.0	21.4	[19]
2.07	13.9	77.3	22.3	[20]
2.15	13.4	80.3	23.2	[21]
2.07	13.9	76.9	22.4 (21.4 certified)	[22]
2.06	13.3	78.3	21.3	[23]
2.10	14.2	77.7	23.2	[24]
2.07	13.0	80.8	21.7	[25]
2.14	14.2	80.7	24.5	[26]
2.10	13.6	77.6	22.3	[27]
2.20	14.2	77.8	24.1	[28]
2.12	14.1	75.0	22.3	[29]
2.09	14.6	79.0	24.1	[30]

2.06	12.7	77.4	20.2	[31]
2.11	13.7	80.1	23.1	[32]
2.15	14.4	81.7	25.2 (24.3 certified)	[33]
2.12	14.7	83.0	25.8 (25.0 certified)	[34]
2.16	15.4	79.4	26.4 (25.7 certified)	[35]
2.13	14.6	82.8	25.9	[36]
2.12	14.3	83.2	25.6 (24.7 certified)	[37]
2.13	14.9	81.9	26.09	This work

REFERENCES

1. J. Lv, Q. Yang, W. Deng, H. Chen, M. Kumar, F. Zhao, S. Lu, H. Hu and Z. Kan, *Chem. Eng. J.*, 2023, **465**, 142822.
2. D. K. Owens and R. C. Wendt, *J. Appl. Polym. Sci.*, 1969, **13**, 1741.
3. J. Lv, X. K. Sun, H. Tang, F. Wang, G. Y. Zhang, L. X. Zhu, J. M. Huang, Q. G. Yang, S. R. Lu, G. Li, F. Laquai and H. L. Hu, *InfoMat*, 2024, **6**, e12530.
4. W. Humphrey, A. Dalke and K. Schulten, *J. Mol. Graphics*, 1996, **14**, 33.
5. T. Lu and S. Manzetti, *Struct. Chem.*, 2014, **25**, 1521.
6. T. Lu and F. Chen, *J. Comput. Chem.*, 2012, **33**, 580.
7. N. Zhao, C. M. Yang, F. G. Bian, D. Y. Guo and X. P. Ouyang, *J. Appl. Crystallogr.*, 2022, **55**, 195.
8. A. Mahmood and J. L. Wang, *Sol. RRL*, 2020, **4**, 2000337.
9. D.-M. Smilgies, *J. Appl. Crystallogr.*, 2009, **42**, 1030.
10. H.-C. Liao, C.-S. Tsao, T.-H. Lin, C.-M. Chuang, C.-Y. Chen, U. S. Jeng, C.-H. Su, Y.-F. Chen and W.-F. Su, *J. Am. Chem. Soc.*, 2011, **133**, 13064.
11. P. Wang, W. Li, O. J. Sandberg, C. Guo, R. Sun, H. Wang, D. Li, H. Zhang, S. Cheng, D. Liu, J. Min, A. Armin and T. Wang, *Nano Letters*, 2021, **21**, 7845.
12. W. Chen, D. Li, X. Chen, H. Chen, S. Liu, H. Yang, X. Li, Y. Shen, X. Ou, Y. Yang, L. Jiang, Y. Li and Y. Li, *Adv. Funct. Mater.*, 2021, **32**, 2109321.
13. S. Qin, C. Lu, Z. Jia, Y. Wang, S. Li, W. Lai, P. Shi, R. Wang, C. Zhu, J. Du, J. Zhang, L. Meng and Y. Li, *Adv. Mater.*, 2022, **34**, 2108829.
14. W. Chen, Y. Zhu, J. Xiu, G. Chen, H. Liang, S. Liu, H. Xue, E. Birgersson, J. W. Ho, X. Qin, J. Lin, R. Ma, T. Liu, Y. He, A. M.-C. Ng, X. Guo, Z. He, H. Yan, A. B. Djurišić and Y. Hou, *Nat. Energy*, 2022, **7**, 229.
15. Y. M. Xie, Q. Yao, Z. Zeng, Q. Xue, T. Niu, R. Xia, Y. Cheng, F. Lin, S. W. Tsang, A. K. Y. Jen, H. L. Yip and Y. Cao, *Adv. Funct. Mater.*, 2022, **32**, 2112126.
16. K. O. Brinkmann, T. Becker, F. Zimmermann, C. Kreusel, T. Gahlmann, M. Theisen, T. Haeger, S. Olthof, C. Tückmantel, M. Günster, T. Maschwitz, F. Göbelsmann, C. Koch, D. Hertel, P. Caprioglio, F. Peña-Camargo, L. Perdigón-Toro, A. Al-Ashouri, L. Merten, A. Hinderhofer, L. Gomell, S. Zhang, F. Schreiber, S. Albrecht, K. Meerholz, D. Neher, M. Stolterfoht and T. Riedl, *Nature*, 2022, **604**, 280.
17. X. Gu, X. Lai, Y. Zhang, T. Wang, W. L. Tan, C. R. McNeill, Q. Liu, P. Sonar, F. He, W. Li, C. Shan and A. K. K. Kyaw, *Adv. Sci.*, 2022, **9**, 2200445.
18. Y. M. Xie, T. Q. Niu, Q. Yao, Q. F. Xue, Z. X. Zeng, Y. H. Cheng, H. L. Yip and Y. Cao, *J. Energy Chem.*, 2022, **71**, 12.
19. Y. Ding, Q. Guo, Y. Geng, Z. Dai, Z. Wang, Z. Chen, Q. Guo, Z. Zheng, Y. Li and E. Zhou, *Nano Today*, 2022, **46**, 101586.
20. C. Wang, W. L. Shao, J. W. Liang, C. Chen, X. Z. Hu, H. S. Cui, C. W. Liu, G. J. Fang and C. Tao, *Small*, 2022, **18**, 2204081.

21. H. Yang, W. Chen, Y. Yu, Y. Shen, H. Yang, X. Li, B. Zhang, H. Chen, Q. Cheng, Z. Zhang, W. Qin, J. D. Chen, J. X. Tang, Y. Li and Y. Li, *Adv. Mater.*, 2022, **35**, 2208604.
22. Q. Yao, Y. M. Xie, Y. Z. Zhou, Q. F. Xue, X. Xu, Y. J. Gao, T. Q. Niu, L. H. Chu, Z. S. Zhou, F. R. Lin, A. K. Y. Jen, T. T. Shi, H. L. Yip and Y. Cao, *Adv. Funct. Mater.*, 2023, **33**, 2212599.
23. H. Wu, T. Chen, Y. Li, S. Guan, L. Zhang, T. Chen, Y. Liu, Y. Jin, L. Zuo, W. Fu, G. Wu and H. Chen, *J. Mater. Chem. A*, 2023, **11**, 6877.
24. S. Q. Sun, X. Xu, Q. Sun, Q. Yao, Y. Cai, X. Y. Li, Y. L. Xu, W. He, M. Zhu, X. Lv, F. R. Lin, A. K. Y. Jen, T. Shi, H. L. Yip, M. K. Fung and Y. M. Xie, *Adv. Energy Mater.*, 2023, **13**, 2204347.
25. X. Lai, S. Y. Chen, X. Y. Gu, H. J. Lai, Y. P. Wang, Y. L. Zhu, H. Wang, J. F. Qu, A. K. K. Kyaw, H. P. Xia and F. He, *Nat. Commun.*, 2023, **14**, 3571.
26. X. Wang, D. Zhang, B. Z. Liu, X. Wu, X. F. Jiang, S. F. Zhang, Y. Wang, D. P. Gao, L. N. Wang, H. L. Wang, Z. M. Huang, X. F. Xie, T. Chen, Z. G. Xiao, Q. Y. He, S. Xiao, Z. L. Zhu and S. F. Yang, *Adv. Mater.*, 2023, **35**, 2305946.
27. Y. Tang, Y. C. Zhang, X. M. Zhou, T. Huang, K. Shen, K. N. Zhang, X. Y. Du, T. T. Shi, X. D. Xiao, N. Li, C. J. Brabec, Y. H. Mai and F. Guo, *Nano Energy*, 2023, **114**, 108653.
28. Y. An, N. Zhang, Z. Zeng, Y. Cai, W. Jiang, F. Qi, L. Ke, F. R. Lin, S. W. Tsang, T. Shi, A. K. Y. Jen and H. L. Yip, *Adv. Mater.*, 2023, **36**, 2306568.
29. G. Xie, H. Li, X. Wang, J. Fang, D. Lin, D. Wang, S. Li, S. He and L. Qiu, *Adv. Funct. Mater.*, 2023, **33**, 2308794.
30. Z. Ma, Y. Dong, R. Wang, Z. Xu, M. Li and Z. a. Tan, *Adv. Mater.*, 2023, **35**, 2307502.
31. W. X. Liu, Y. X. Duan, Z. W. Zhang, J. X. Gao, S. X. Li, Z. Fink, X. F. Wu, Z. F. Ma, A. Saeki, T. P. Russell and Y. Liu, *ACS Energy Lett.*, 2023, **8**, 4514.
32. S. S. Mali, J. V. Patil, J. A. Steele, M. K. Nazeeruddin, J. H. Kim and C. K. Hong, *Energy Environ. Sci.*, 2024, **17**, 1046.
33. S. Wu, Y. Yan, J. Yin, K. Jiang, F. Li, Z. Zeng, S.-W. Tsang and A. K. Y. Jen, *Nat. Energy*, 2024, **9**, 411.
34. Z. Zhang, W. Chen, X. Jiang, J. Cao, H. Yang, H. Chen, F. Yang, Y. Shen, H. Yang, Q. Cheng, X. Chen, X. Tang, S. Kang, X.-m. Ou, C. J. Brabec, Y. Li and Y. Li, *Nat. Energy*, 2024, **9**, 592.
35. X. Jiang, S. C. Qin, L. Meng, G. R. He, J. Y. Zhang, Y. Y. Wang, Y. Q. Zhu, T. W. Zou, Y. F. Gong, Z. K. Chen, G. P. Sun, M. C. Liu, X. J. Li, F. L. Lang and Y. F. Li, *Nature*, 2024, **635**, 860.
36. S. Q. Kang, Z. Y. Wang, W. J. Chen, Z. C. Zhang, J. L. Cao, J. L. Zheng, X. X. Jiang, J. C. Xu, J. X. Yuan, J. Zhu, H. Y. Chen, X. N. Chen, Y. W. Li and Y. F. Li, *Adv. Mater.*, 2024, **n/a**, 2411027.
37. X. Wu, D. Zhang, B. Liu, Y. Wang, X. Wang, Q. Liu, D. Gao, N. Wang, B. Li, L. Wang, Z. Yu, X. Li, S. Xiao, N. Li, M. Stolterfoht, Y.-H. Lin, S. Yang, X. C. Zeng

and Z. Zhu, *Adv. Mater.*, 2024, **n/a**, 2410692.